

Three-dimensional finite element analysis of single-turn coil systems

D.F. Rankin, B.M. Novac and I.R. Smith

Abstract: The paper describes a multiphysical finite-element approach to the three-dimensional modelling of metallic structures that are transiently subjected to heavy electromagnetic loading, as in the metal forming industry. Electromagnetic, thermal and structural effects are all taken into account, and very good agreement is obtained in detailed comparisons with measurements from non-destructive experiments. Acceptable agreement also exists in the peak field prediction of destructive experiments, in which single-turn coils are used to generate ultrahigh magnetic fields, typically for use in solid-state experimental physics.

1 Introduction

Although the study of pulsed power originated in the 1960s, in answer to many warfare requirements, the technology has subsequently been expanded and developed in a large number of industrial and scientific applications. Metal forming [1] is an advanced technology that employs the very considerable power generated during an electromagnetic implosion to obtain metal products in a variety of complex shapes. A number of European universities (mostly in Germany) are collaborating with industrial partners in developing the detailed numerical models required for the optimisation of these industrial processes [2, 3].

Work on developing a complete, multiphysical, three-dimensional (3D) model is underway at Loughborough University in the UK [4], and this paper presents the most relevant results achieved during the first phase of the project. A z-pinch geometry is commonly adopted in industrial processes, but, in the application for which the model is required, the geometry is quite different, and there is clearly a need for the code to be benchmarked against reliable experimental data in which 3D deformation is present. The electromagnetic implosion facility at Loughborough enables thin metal liners to be accelerated to high speeds using θ -pinch geometry [5], but the liner is destroyed during the implosion and the data obtained from flash x-rays or high-speed cameras are not sufficiently detailed to allow immediate benchmarking of the model. As the development of a 3D model is an extremely demanding task, a simpler preliminary phase of the work was devoted to the dynamics of a thick single-turn coil carrying the very large current generated during the discharge of a high-energy capacitor bank.

After a description of the 3D model, the code is benchmarked against a specially designed, non-destructive

single-turn coil experiment. Following this, and to investigate the limitations of the model, predicted results are compared with data obtained from destructive experiments generating ultrahigh magnetic fields and employing smaller single-turn coils. Based on the evidence of this work, ways to improve the 3D code are suggested.

2 Multiphysical FEA modelling

Three-dimensional finite element analysis (FEA) can be used to provide an accurate description of the complex physical processes that occur during pulsed electromagnetic loading of an electrical conductor. The analysis to be presented here employs a commercially available code (ANSYS Multiphysics) and adopts a multiphysical approach. The three main disciplines involved are electromagnetic (EMAG), thermal (THERM) and structural (STRUCT), and these must be solved independently and consecutively throughout a computational solution. During the solution, numerical results from one discipline are passed as loads to the next, as shown in the flow chart of Fig. 1. The symbol K indicates the number of specific time intervals that have elapsed and is incremented after each iteration cycle throughout the solution. The solution ends when K reaches a specified maximum, signifying the end of the period of interest.

Within the EMAG environment, a simple lumped circuit representation of the electrical energy supply circuit is connected to an FEA model of the load to be analysed (a metallic structure), so as to establish the FEA model as a component of the circuit. This overall representation models the capacitor discharge through the transmission line feeding the network and supplies the source current density vector to a magnetic vector potential in the FEA model. Over a specified time step, the magnetic field and current distributions, Joule energy and nodal Lorenz forces are all calculated, as are the total FEA model inductances and resistances. All this information is saved within an EMAG database to be retrieved in the next EMAG iteration.

Within the THERM environment, the discretisation of elements is maintained as in the EMAG environment, allowing the direct transfer of nodal solutions/loads from one environment to the next. Joule energy deposition evaluated within the EMAG solution is passed directly to

© The Institution of Engineering and Technology 2006

IEE Proceedings online no. 20050081

doi:10.1049/ip-smt:20050081

Paper first received 7th November 2005 and in final revised form 6th February 2006

The authors are with the Department of Electronic & Electrical Engineering, Loughborough University, Loughborough, Leicestershire, LE11 3TU, UK
E-mail: i.r.smith@lboro.ac.uk

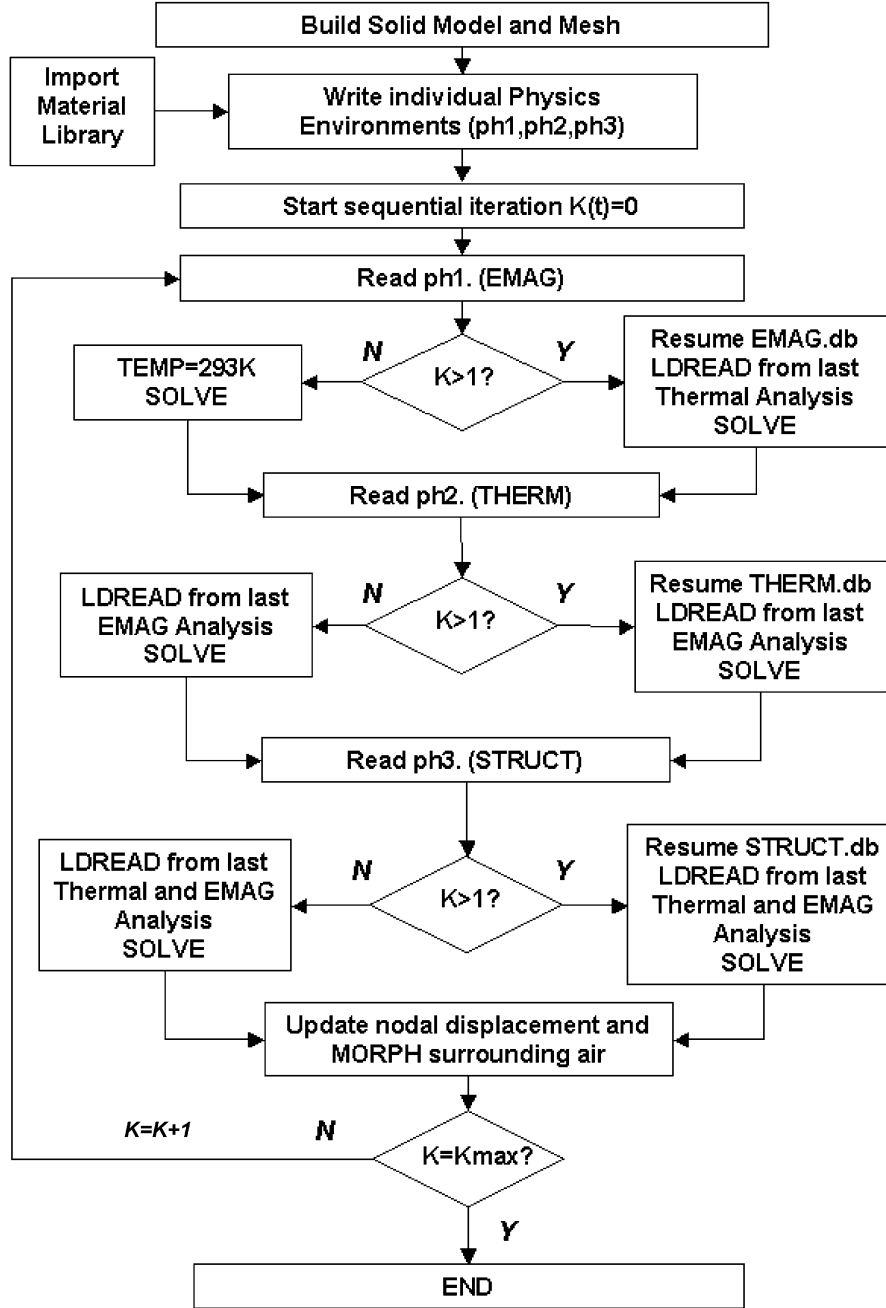


Fig. 1 Multiphysical flow chart

the THERM nodes, and, with appropriate time stepping and material modelling, the temperature rises are determined, together with the associated conductive heat flux gradient. These data are again stored so that the solution can be continued at the next iteration. Radiation losses are neglected, as these play an insignificant role in the thermal losses in the application considered later.

The same discretisation is maintained in the STRUCT environment. Lorenz nodal solutions from EMAG and temperature solutions from THERM are applied to the STRUCT model. In the structural solution, the nodal displacements are determined and used to modify the location of the active nodes contained in the element matrix for all three databases. The complete solution is iteratively modelled throughout each environment at suitable time steps.

Although two-dimensional modelling is obviously possible, the present paper concentrates on a more complete 3D approach.

3 Comparison with experimental data

It is very difficult to obtain accurate data relevant to all three physical disciplines involved in the multiphysical modelling from experiments in which a metallic structure is subjected to intense electromagnetic loading by the passage of large electric currents. One of the simplest arrangements that presents a 3D aspect is the single-turn coil (STC). Figure 2 presents a typical STC arrangement, including the equivalent electrical circuitry involved.

Switch S of Fig. 2 is closed when the high energy capacitor bank C is charged to an initial high voltage V_0 , to discharge the electrostatically stored energy into the coil through the flat parallel-plate transmission line of inductance L_T and resistance R_T . The resulting current I_C rises rapidly and eventually produces a high magnetic flux density at the centre of the STC that is related to the energy initially stored and the geometric size of the system and is inversely related to the overall inductance of the circuit.

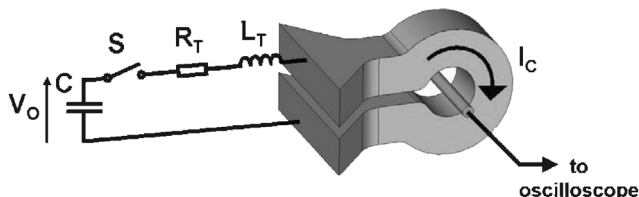


Fig. 2 Experimental STC arrangement

R_T and L_T include all circuit resistances and inductances other than STC

During an experiment, the electromagnetic Maxwell tensor (magnetic pressure) acts on the STC, producing 3D deformation.

Insulation provided by Mylar polyester film separates the two plates of the transmission line, and powerful clamps restrict their movement during the capacitor discharge. Design E1 in Table 1 details the main experimental parameters of an STC validation experiment at Loughborough.

The typical topology and the way in which the FEA model is established are shown in Fig. 3. Figure 3a depicts a topological representation of an STC as shown in Fig. 2. This solid model can, however, be simplified by taking advantage of the inherent degrees of symmetry. Symmetry exists in this model in two of the planes shown in the coordinate system in Fig. 3. First, symmetry exists in the $x-y$ plane, and, secondly, geometric symmetry exists in the $x-z$ plane; thus the model can be reduced by the discarding from calculations of the lower and left hand section of the model, as shown in Fig. 3b.

Figures 3b and c show the simplified STC solid model used at Loughborough in FEA simulation. The geometrically reduced model, as presented above, allows for a reduction in overall FEA degrees of freedom (unknowns) and, hence, a reduction in the overall matrix sizes and therefore also the computational run-time. However, to achieve this, suitable ‘boundary conditions’ must be established. Considering the EMAG environment, the solution must be aware that symmetry is to be considered across the $x-y$ plane (SYMM-1), but ‘anti-symmetry’ is to

Table 1: Data for Loughborough STC experiments. All STCs made from copper

Design	Coil geometry			External circuitry			
	inner radius, mm	outer radius, mm	axial length, mm	C , μF	V_o , kV	R_T , m Ω	L_T , nH
E1	10.1	12.1	40.7	210.6	13.7	0.5	20.0
E2	1.0	2.0	2.0	56.6	25.3	7.0	18.0
E3	1.5	2.5	4.9	56.6	25.0	9.0	19.1

E1: non-destructive experiment; E2 and E3: destructive experiments

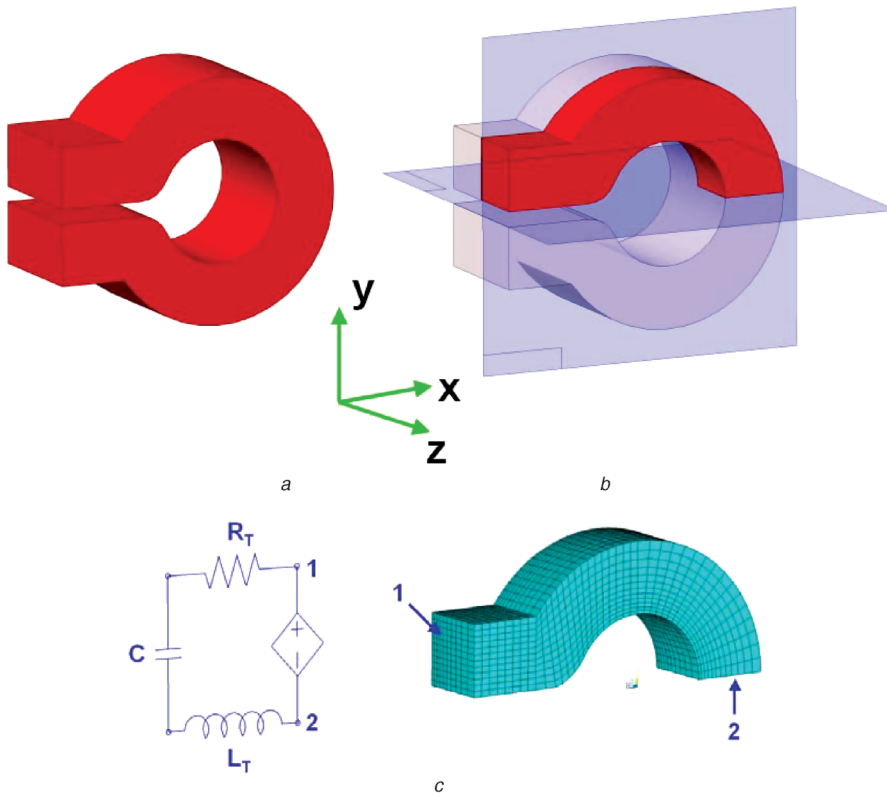


Fig. 3 STC model

a Full solid model

b Quarter model used at Loughborough

c FEA model

be considered across the x - z plane (SYMM-2). Thus, if we consider the current vector within the model, it is clear that, through SYMM-1, the current will reflect magnitude and direction across the line of symmetry; however, in SYMM-2, although the magnitude will be the same, the direction will be reversed. Hence, in the upper coil, current flows in, and, in the lower (un-modelled) coil, current would flow out.

In Fig. 3c, a meshed volume is shown of the quarter-coil and highlights the attachment to the FEA circuit model used in the electromagnetic analysis. By establishing the correct boundary conditions, as mentioned above, the circuit is able to compute the overall resistance and inductance as if it were connected to the entire model of Fig. 3a. The mesh shown in Fig. 3c is for clarity; however, in reality, surrounding the coil is an air mesh that includes far-field elements on the outer boundary. These far-field elements model the infinite plane.

Preliminary experimentation was obviously necessary to tune the parameters of the STC and therefore to allow the full post experimental geometric shape of the STC to be compared with that predicted. Preliminary modelling helped to define coil conditions so as to avoid completely the solid–liquid phase transition during the experiment and, hence, material flow or loss during the experiment. Flux density measurements were made at the coil centre using magnetic pick-up probes together with auxiliary circuits and equipment similar to those described elsewhere [5]. For experiment E1, the probe had a three-turn coil wound on a 3 mm diameter ceramic mandrel. The probe was calibrated as described in [5], with the measurement error thought to be less than 3%. The measured and FEA-predicted variations in the flux density during the experiment are compared in Fig. 4 and can be seen to agree at all times to within the experimental error.

Measured and predicted final forms of the STC are compared in Fig. 5, with the photograph of Fig. 5a showing the flanged shape of the STC recovered after the experiment for which the magnetic field history is recorded in Fig. 4. Owing to the magnetic field diffusion process generating a current distribution with peaks located at the outer edge of the STC, the combined electromagnetic stress and thermal effects have caused the material to become plastic and to deform outwardly, mainly at these edges. Figure 5b shows a simulation of the final shape of the deformed STC coil, 150 μ s after closure of switch S, and this clearly corresponds extremely well to the actual shape of the recovered STC. Measurements show that the actual central inner radius of 11.4 mm is simulated as 11.1 mm. Similarly, the measured radius and axial length at the point highlighted by the

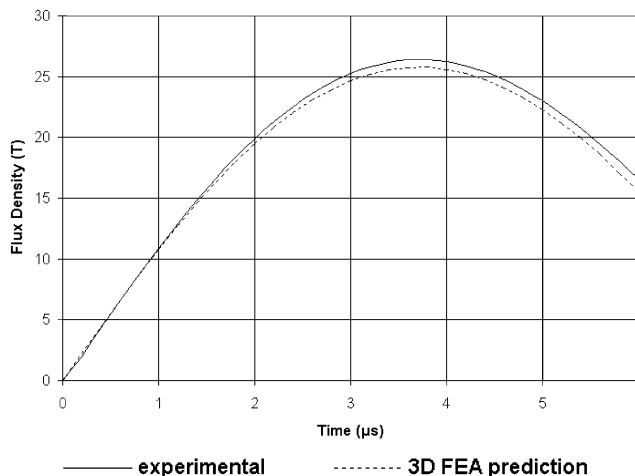


Fig. 4 Axial magnetic flux density of coil E1

arrows in Fig. 5a are, respectively, 17.1 mm and 34 mm, which again compare well with corresponding measurements from the simulation of 17.2 mm and 32.8 mm. All other measurements of the actual geometric translations agree with those simulated to within the same degree of accuracy.

The deformation is most pronounced diametrically opposite the gap where the current enters and leaves the STC, and Fig. 6 shows 3D predictions of the displacement and associated velocity of the radius and axial length at this point. Predictions show that the edge of the coil has come to a complete rest after about 150 μ s from the start of the current discharge, and this can be taken as indicative of the coil as a whole.

It can also be seen from Fig. 6 that, when the peak field occurs after 3.8 μ s (see Fig. 4), the outer rim has already expanded by almost 0.1 mm and is travelling at a speed of 100 m s $^{-1}$. The dimensions of the STC are therefore changing very rapidly.

The 3D model enables the induced stress distribution within the STC to be observed and any potential structural weaknesses to be highlighted. Figure 5c presents a Von Mises stress plot when the coil has finally come to rest, with the copper being annealed after construction. As expected, Fig. 5c shows that significant areas of stress are evident at both the outer flanges of the STC and in the clamping regions where it joins the transmission system. Although stress is translated across the centre of the coil, this does not happen homogenously, and it can also be seen in Fig. 5c that there are areas of high stress concentration. These areas are separated by areas of much lower stress, and, if the STC was subjected to a greater deforming energy, these regions would clearly be the first to fracture.

Figure 7 presents spatial distributions after 150 μ s of the temperature, Joule heating and current density throughout the STC, with the highest temperatures around the inner side of the flanges and where the transmission line meets the coil.

During the simulation, relevant temperature-dependent material properties for each individual environment are used. As the temperature approaches that of melting through to vaporisation, data from the SESAME [6] database allow for prediction of conductivity within the EMAG environment. Similarly, the temperature-dependent variation in enthalpy allows for the consideration of latent heat absorption with the THERM environment. However, phase changes were not considered within the STRUCT environment. At these absolute extremes, the simplifications are an inherent limitation when this integrated code is implemented. However, the results in Fig. 7 highlight the breadth and quality of information that is available, by pinpointing the magnitude and location of such quantities from the simulation.

4 Destructive ultrahigh magnetic field experiments

Results obtained from a series of non-destructive experiments similar to that described previously were used to benchmark the present 3D code. A number of important issues related to the limitations of the model, however, remain unanswered, and these may become important in future applications, should accidental overloading of a metallic structure cause part of it to be melted (or even vaporised) and partially (or completely) destroyed. The physics of the code does not include high-energy/high-temperature phenomena related to the non-linear diffusion of strong magnetic fields producing surface vaporisation,

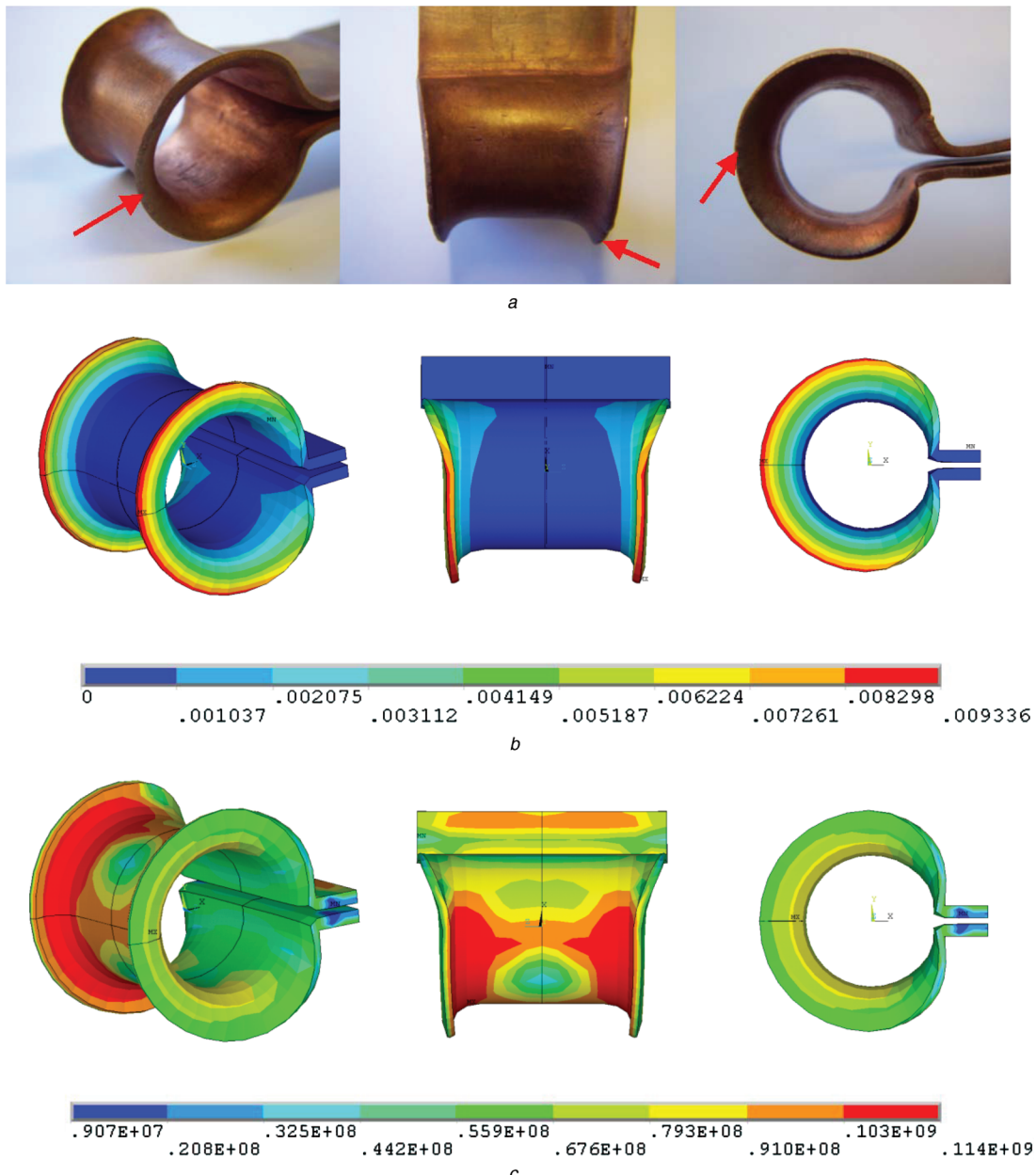


Fig. 5 Deformed coil E1

a Recovered test piece

b Predicted shape, vector displacement in m
c Von Mises stresses, isocontours in N m^{-2}

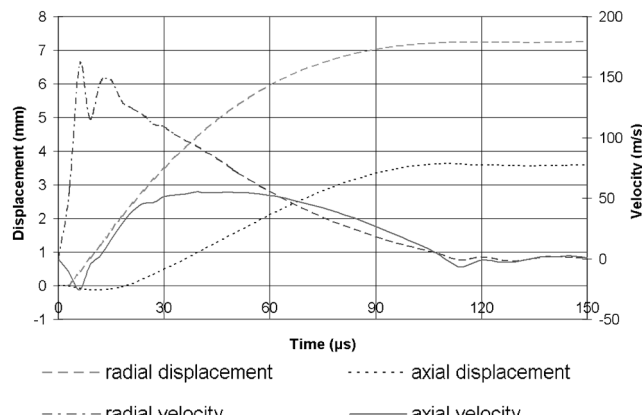


Fig. 6 Predicted dynamics of coil E1

shock waves etc. Nevertheless, to establish the limitations of the code, a number of experiments at these extremes were modelled, in which small-size STCs were subjected to very high current loading. Aided by the coil inertia, such experiments are traditionally performed to produce, for a very short time, but very reproducibly, ultrahigh magnetic fields of hundreds of Teslas (a few MG) in the small central volume, in applications mostly related to solid state physics [7, 8].

Data for two such experiments performed at Loughborough are given as sets E2 and E3 in Table 1. As presented elsewhere [5, 9], either magnetic pick-up probes or Faraday rotation sensors were used to record accurately the flux density produced on the axis of the coil, with recordings made on a 500 MHz, 5 GS s^{-1} digital storage oscilloscope. Comparison is made between the results from these extreme destructive experiments (i.e. the coil is irrecoverably destroyed at the end of the experiment) and the 3D STC model described above.

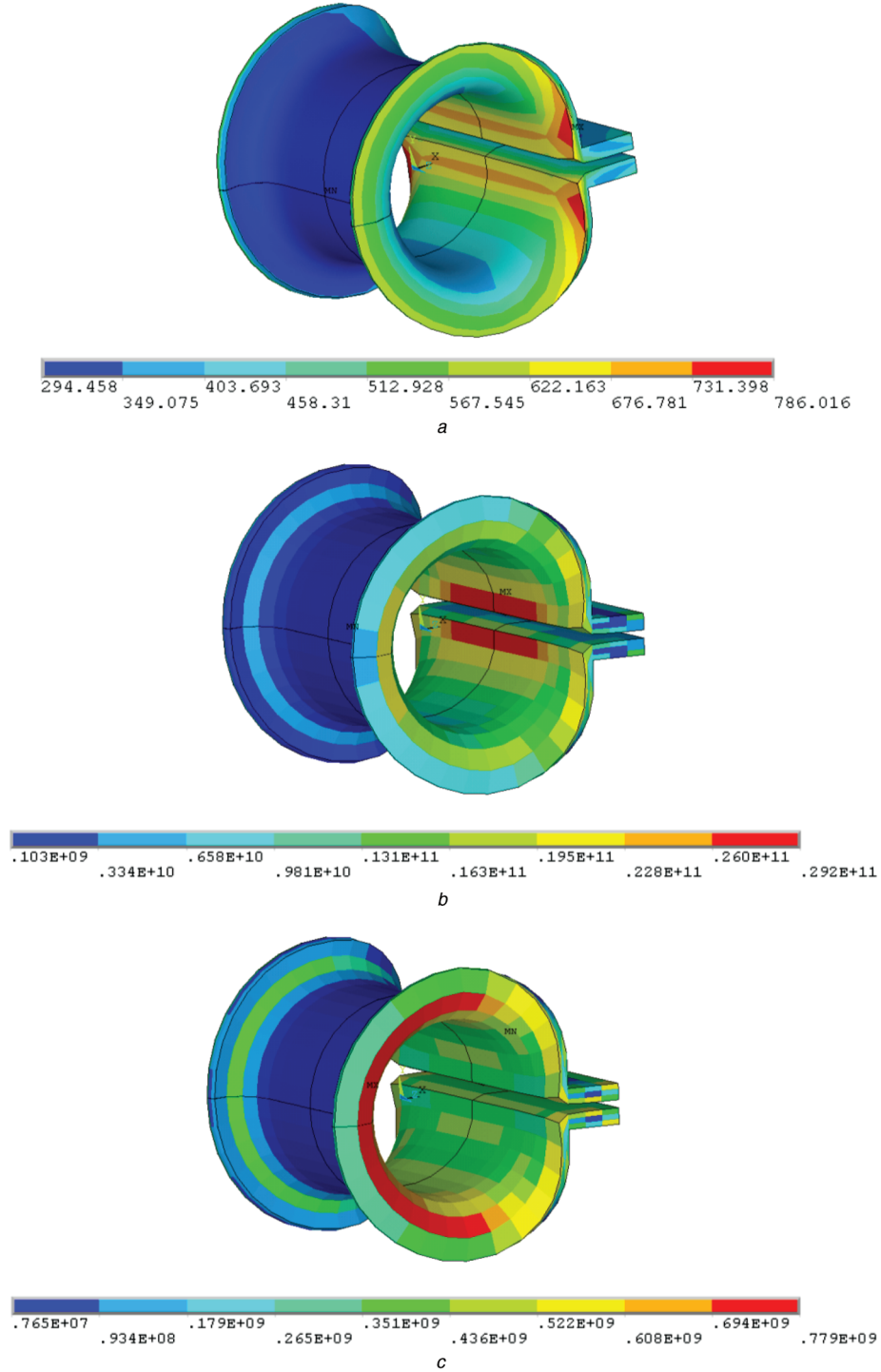


Fig. 7 3D FEA spatial distribution within coil E1

- a Temperature, K
- b Joule heating, J
- c Current density, A m^{-2}

By employing a flash X-ray source, it is also possible to observe the deformation of the destructive system throughout the lifetime of the coils.

Figure 8 compares the measured and predicted 3D time variation of the flux density on the axis of coil E2. The flux density in the central region of the STC is measured by a magnetic pick up probe having two turns on a 1 mm diameter mandrel and having an estimated calibration error of less than 3%. The peak flux density of 240 T occurs about 0.8 μs after closure of the switch S.

The 3D code shows that the maximum flux density and the time at which it occurs are predicted to within 2% of the

experimental data, which is close to the experimental error introduced by the probe. Owing to its relatively large cross-sectional area, the calculation accounted for spatial variations of the flux density within the pick-up probe itself.

The X-ray pictures in Fig. 9a show an end view of coil E2 prior to the capacitor discharge (left) and 820 ns after switch S is closed (right), very near to the time when the maximum central flux density is produced (see Fig. 8). It is evident that, owing to the magnetic pressure generated, the coil has started to expand radially. However, the expansion is not homogenous, with the area highlighted by the arrow A in

Fig. 9a travelling furthest in this time. Also obvious throughout the Figure is a widening of the gap in the coil at the connection to the transmission system and some necking of the coil in the lower left section after 820 ns,

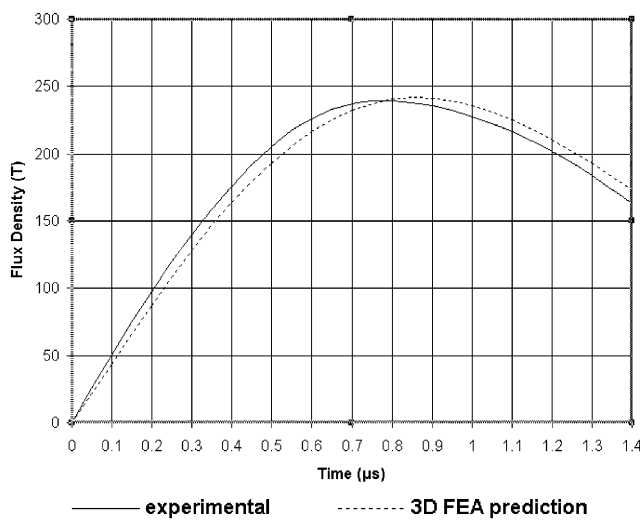


Fig. 8 Axial magnetic flux density of coil E2

probably owing to initial inhomogeneity in the cross section of the coil.

In Fig. 9b, predicted end views of the coil are superimposed on the experimental recordings, and the correlation is acceptable. The darkened line around the top of the FEA coil after 820 ns is due to the radial expansion at the centre of the coil being slightly greater than it is at the end, something that, to be fully observed, normally requires two X-ray pictures taken at a right-angle. Necking is not apparent in Fig. 9b, owing to the initially uniform cross-section.

Figure 10 shows the predicted radial and axial length dynamics of the coil at the point highlighted by the arrow A in Fig. 9a. At the time of peak field, the outer edges have translated almost 0.34 mm radially, reaching predicted speeds in excess of 1500 m s^{-1} .

There are clearly limitations to prediction of the destructive experiment when large thermal and structural instabilities (shock waves, phase transitions) are present beyond a certain time. Thus Fig. 11 shows an X-ray image of a coil identical to coil E2, obtained 1200 ns after the initial switch is closed. The X-ray highlights the explosive petalling effect that is certainly beyond the capabilities of the current 3D model. However, this occurs at a time far beyond that at which the peak field is produced (see Fig. 8).

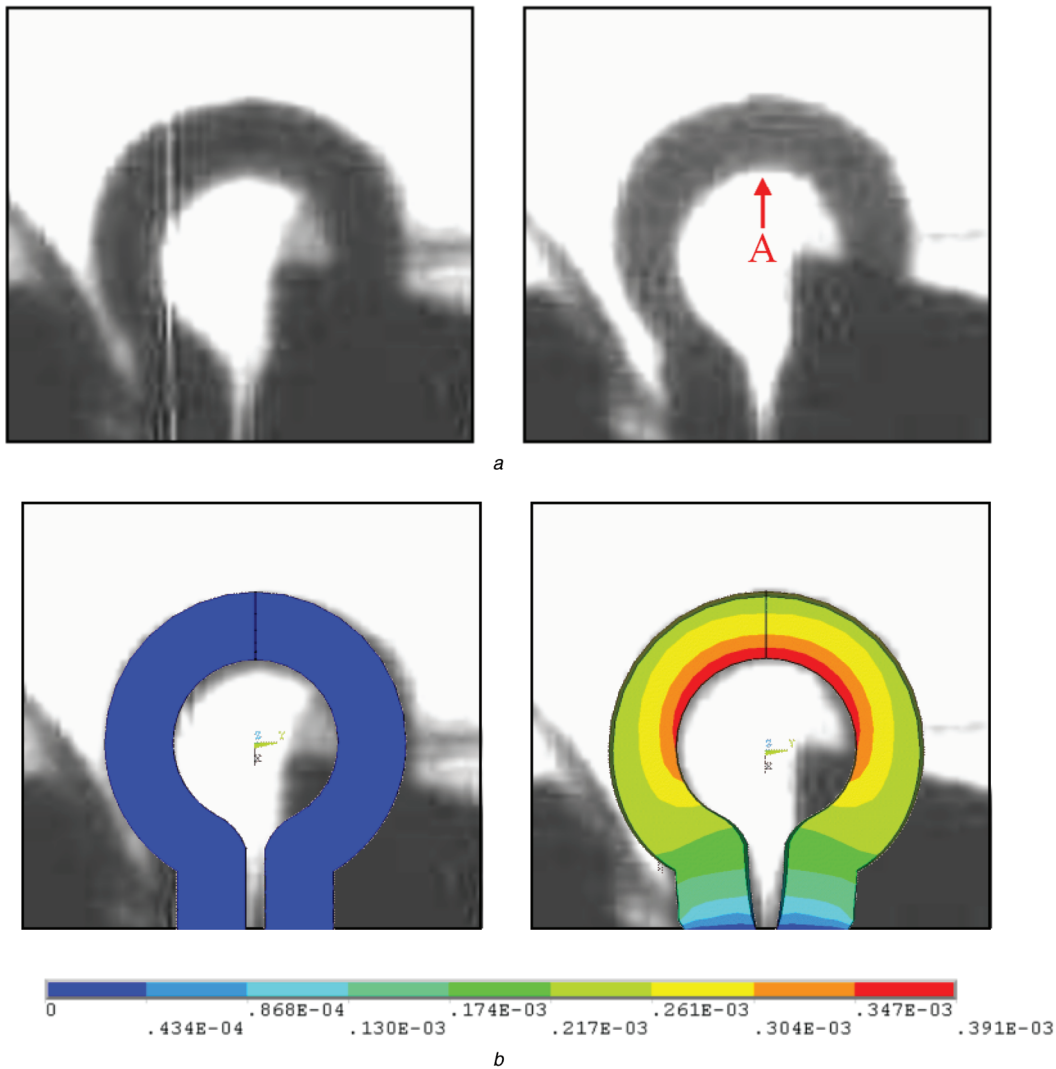


Fig. 9 X-ray dynamics coil E2

a Images at 0 ns and 820 ns

b Corresponding predicted shapes; scale indicates vector displacement in metres

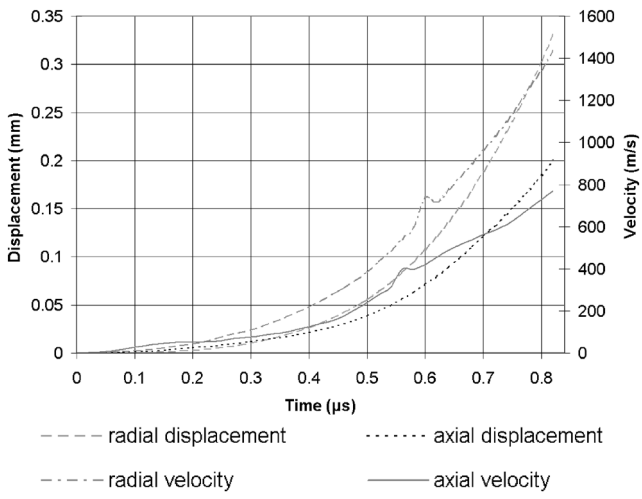


Fig. 10 Predicted dynamics of coil E2

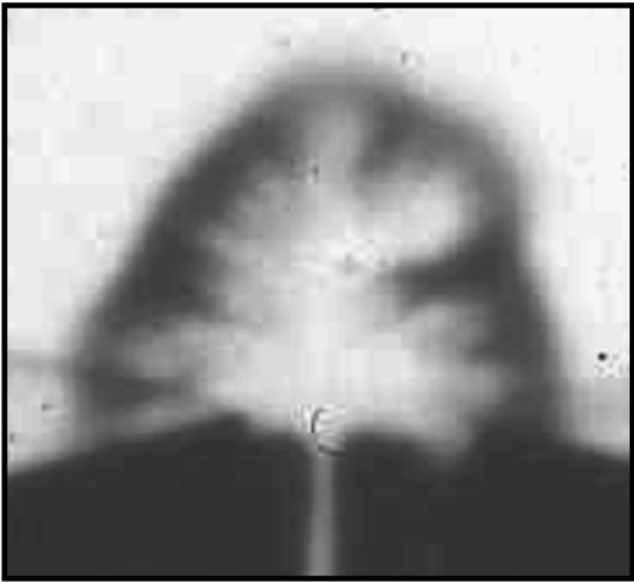


Fig. 11 X-ray dynamics of coil E2 at 1200 ns

For the experiment with coil E3 in Table 1, the mean flux density along the central axis of the STC was measured using a Schott SF6 high-lead glass Faraday rotation sensor, 5 mm long and 1.5 mm^2 in cross-section. The cross-section of the laser beam through the crystal was reduced by a two-lens system, with the maximum intensity focussed on a circular region about 0.1 mm in diameter. As, however, it is difficult to estimate the influence of light outside this region, the active cross-section in which the magnetic field contributes to the Faraday rotation was conservatively estimated as a circle 0.3 mm in diameter, and it is clear that the predicted magneto-optic effect will therefore always be less than the measured figure. Figure 12 compares both the measured and predicted output signals from the probe and the corresponding axial flux densities derived from the Faraday rotation signal. The predicted output signal takes full account of both the axial and radial flux density distribution within the crystal.

The maximum axial flux density of 140 T is produced within $1.25 \mu\text{s}$ of the switch closure, in a greater volume than that of coil E2, and the 3D model predicts 129.5 T, at the same time. In all cases, the accuracy of prediction is within 7%, although, most probably, shock waves would

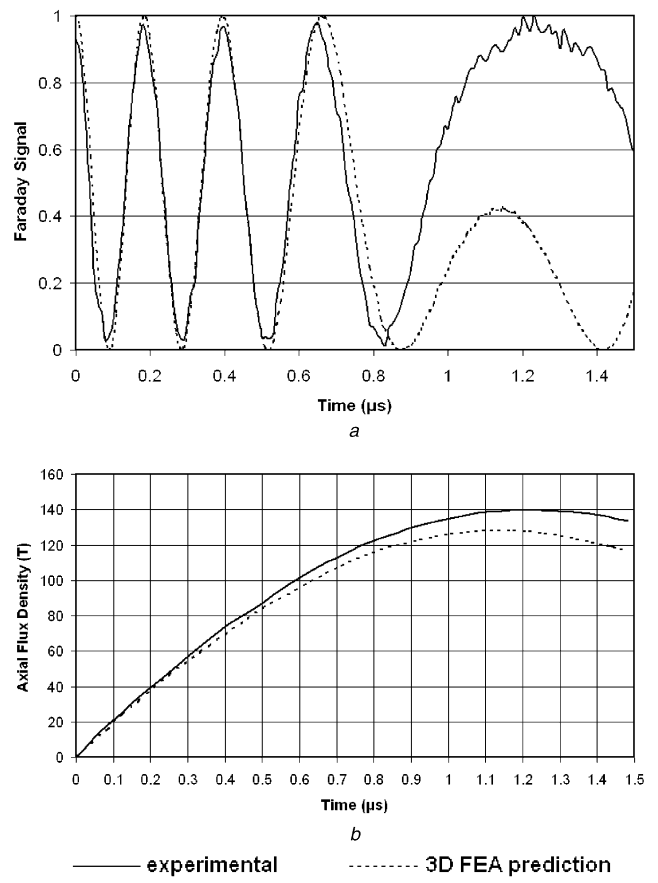


Fig. 12 Coil design E3
a Faraday rotation signal (in arbitrary units)
b Axial magnetic flux density

have affected the crystal in the final 200 ns before the peak field was produced.

5 Conclusions

It has been demonstrated that accurate 3D modelling of metallic structures (such as a STC) under heavy transient electromagnetic loading is possible using FEA. In particular, it has been shown that 3D elasto-plastic flow, essential in a number of applications, can be accurately modelled.

A major benefit from 3D FEA modelling is the wealth of information that then becomes available. Electromagnetic, thermal and structural data can all be deduced at any given point in time, without the dimensional simplifications common in other simplified filamentary models [10, 11]. It is clear, however, that significant limitations still exist when ultra-magnetic fields are considered. There is a need for more accurate material data for use in high-power systems such as destructive experiments E2 and E3, where extreme conditions are expected. At present, certain data are unreliable in this high temperature/high pressure region, which can considerably influence the theoretical predictions. This is of paramount importance when the model is applied to θ or Z -implosions at MA levels of current.

The ability to work in three dimensions allows for quick problem isolation and system innovation, as well as providing a deeper understanding of the system as a whole. The 3D FEA work at Loughborough is now expanding into other ultrahigh pulsed power systems such as electromagnetic flux compression.

6 References

- 1 Kristiansen, M.: 'Pulsed power applications'. 9th IEEE Int Pulsed Power Conf., Albuquerque, New Mexico, 1993, pp. 6–10
- 2 Schatzing, W., Wollenberg, G., Zange, R., and Scheibe, H.P.: 'Calculations of the transient magnetic fields of coil configurations for magnetic forming'. Int Conf on Pulsed Power Applications, Gelsenkirchen, Germany, 2001, E10/1–4
- 3 Psyk, V., Beerwald, C., Kleiner, M., Beerwald, M., and Henselek, A.: 'Use of electromotive forming in process combinations for the production of automotive parts'. 2nd European Pulsed Power Symp, Hamburg, Germany, 2004, pp. 82–86
- 4 Rankin, D.F., Novac, B.M., and Smith, I.R.: 'Two and three dimensional multiphysical modelling of high field solenoid experiments by finite element analysis'. Proc. of the Tenth Int. Conf. on Megagauss Magnetic Field Generation and Related Topics, Berlin, Germany, 2005, pp. 313–316
- 5 Novac, B.M., Smith, I.R., Rankin, D.F., and Hubbard, M.: 'A fast and compact θ -pinch electromagnetic flux-compression generator', *J. Phys. D: Appl. Phys.*, 2004, **37**, pp. 3041–3055
- 6 Lyon, S.P., and Johnson, J.D.: 'SESAME. The Los Alamos National Laboratory equation of state database', 2002, Report LA-UR-92-3407
- 7 Portugall, O., Puhlmann, N., Muller, H.U., Barczewski, M., Stolpe, I., and Van Ortenberg, M.: 'Megagauss magnetic field generation in single-turn coils: new frontiers for scientific research', *J. Phys. D: Appl. Phys.*, 1999, **32**, pp. 2354–2366
- 8 Miura, N., Matsuda, Y.H., Uchida, S., Goto, T., Mitamura, H., Osada, T., and Ohmichi, E.: 'New megagauss laboratory of ISSP at Kashiba', *Physica B*, 2001, **294–295**, pp. 652–567
- 9 Novac, B.M., and Smith, I.R.: 'Preliminary experimentation on a flux-compression microwave source'. European Pulsed Power Symp., St Louis, France, 2002, pp. 7/1–7/6
- 10 Miura, N., and Nakao, K.: 'Computer analysis of megagauss field generation by condenser bank discharge', *Jap. J. Appl. Phys.*, 1990, **29**, pp. 1580–1599
- 11 Novac, B.M., Smith, I.R., and Hubbard, M.: '2-D modelling of electromagnetic flux-compression in θ -pinch geometry', *IEEE Trans. Plasma Sci.*, 2002, **32**, pp. 1896–1901